Imaging the Dynamics of Reactions between Cl Atoms and the Cyclic Ethers Oxirane and Oxetane

Julie K. Pearce, Bertrand Retail, Stuart J. Greaves, Rebecca A. Rose, and Andrew J. Orr-Ewing*

School of Chemistry, University of Bristol, Cantock's Close, Bristol BS8 1TS, United Kingdom

Received: September 13, 2007

Direct current slice velocity map ion images of the HCl($v' = 0$, J') products from the photoinitiated reactions of ground state Cl atoms with ethane, oxirane (c-C_2H_4O), and oxetane (c-C_3H_6O), at respective mean collision energies of 5.5, 6.5, and 7.3 kcal mol^{-1}, were analyzed using a Legendre moment fitting procedure. The experimental method and the fitting technique were tested by comparing the derived center-of-mass (CM) frame angular scattering distribution for the HCl($v' = 0$, $J' = 1$) products from the reaction of Cl + C_2H_6 with those determined by Suits and co-workers from a crossed molecular beam experiment. For the Cl + c-C_2H_4O reaction, a broad, forward, and backward peaking CM frame angular distribution of HCl($v' = 0$, $J' = 2$) products was determined, with an average fraction of the available energy released as product translational energy of $\langle f_t \rangle$, equal to 0.52 ± 0.18. The HCl consumes only 1% of the available energy, and conservation arguments dictate that the radical coproduct is significantly internally excited, corresponding to an average fraction of the available energy of $\langle f_{int}(c\text{-}C_2H_3O) \rangle$, equal to 0.47 ± 0.18. For the reaction of oxetane with Cl atoms, abstraction of H atoms is possible from carbon atoms from positions either α or β to the O atom. The contributions to the reaction from these two H-atom abstraction channels were estimated to be 63 and 37%, consistent with an unbiased propensity for removal of α- and β-H atoms that are present in 2:1 abundance. The angular scatter of products in the CM frame is also broad and forward−backward peaking and is reminiscent of the products of the Cl + CH_3OH and CH_3OCH_3 reactions. The derived mean fraction of the available energy channelled into product translation is $\langle f_t \rangle = 0.54 \pm 0.12$ for each of the two abstraction pathways. With only a small amount of energy in the rotation of the HCl($v' = 0$), the remainder is accounted for by excitation of the radical coproduct internal modes, with $\langle f_{int}(c\text{-}C_3H_5O) \rangle = 0.42 \pm 0.12$ for both α- and β-H abstraction. The broad product scattering in the CM frame observed for both reactions of Cl atoms with the cyclic ethers is consistent with reactive collisions over a wide range of impact parameters, as might be expected for barrierless reactions with loose transition states.

1. Introduction

Numerous recent experimental and computational studies are rapidly establishing the reactions of Cl atoms with various organic molecules—most notably methane—as paradigms for the dynamics of bimolecular reactions involving polyatomic molecules.[1,2] The earliest of these investigations focused on Cl atom reactions with alkanes,[3−12] but their scope has since been widely extended to include the dynamics of reactions of a variety of functionalized organic molecules.[1,13−22] Ionization of the HCl or organic radical products, either by vacuum ultraviolet (UV) light or resonance-enhanced absorption of multiple UV photons, coupled with time-of-flight mass spectrometry (TOF-MS) and velocity map ion imaging,[2,23−29] has proven to be a powerful combination for the determination of center-of-mass (CM) frame-scattering distributions, in some cases with quantum-state specificity.[18,19,25,26,30−34] Similar methods are increasingly being applied to the detailed study of the mechanisms of further bimolecular reactions.[29,35]

A variety of structural motifs are available for small organic molecules, including straight-chain, branched, and cyclic arrangements of the constituent atoms. These molecules thus provide opportunities to explore the effects of the shape, polarity, and internal degrees of freedom of reagents and products on reactive scattering dynamics. Previous experiments on the dynamics of Cl atoms with the cyclic ethers oxirane (c-C_2H_4O) and oxetane (c-C_3H_6O) and the cyclic thio-ether thiirane (c-C_2H_4S) found the extent of rotational excitation of the HCl products to be lower than expectations based on correlations with the dipole moments of the radical coproduct.[2,21] These correlations were derived from outcomes of reactions of Cl atoms with a series of noncyclic alcohols, ethers, and alkyl halides and were attributed to anisotropy in the post-transition state (TS) regions of the potential-energy surfaces (PESs) for these reactions.[13,14,16,17] Trajectory calculations demonstrated that significant reorientation of the radicals could occur on the time scale of the separation of these and the HCl products of reactive encounters, with consequent torque on the HCl induced by electrostatic interactions such as those arising from the dipole moments of both polar products. The different reorientation dynamics of the near-oblate cyclic radicals were argued to disfavor the separating products from finding geometries associated with the attractive post-TS interactions, with the HCl consequently experiencing a lower torque. In this paper, we revisit the dynamics of reaction of the two cyclic ethers with

* To whom correspondence should be addressed. E-mail: a.orr-ewing@bris.ac.uk. Phone: +44 117 928 7672. Fax: +44 117 925 0612.

10.1021/jp0773684 CCC: $37.00 © 2007 American Chemical Society
Published on Web 12/01/2007

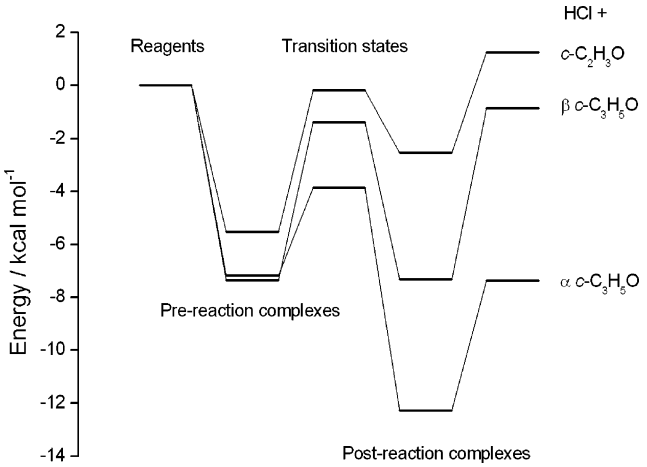

Figure 1. Relative ab initio energy profiles based upon 0 K calculated energies of reactants, products, molecular complexes, and transition states for the Cl + *c*-C_2H_4O and Cl + *c*-C_3H_6O reactions. The energies were calculated at the G2//MP2/6-311G(d,p) level of theory and include zero-point corrections.

Cl atoms and report the CM frame scattering of the products. Comparisons are drawn with the reactions of Cl atoms with methanol and dimethyl ether (DME).[14] Further measurements of the benchmark reaction of Cl atoms with ethane

$$Cl + C_2H_6 \rightarrow HCl + C_2H_5$$
$$\Delta_r H_{298K} = -2.08 \pm 0.39 \text{ kcal mol}^{-1} \quad (1)$$

for which CM frame-scattering distributions are available from crossed molecular beam (CMB) experiments[36,37] serve as a test of the experimental procedure and the methods of data analysis.

Stationary points along the reaction coordinates of the studied reactions are shown in Figure 1, with the energies derived from electronic structure calculations performed at the G2//MP2/6-311G(d,p) level of theory. The reaction of Cl with oxirane is shown in the figure to proceed via H atom abstraction to give HCl and the cyclic oxiranyl (*c*-C_2H_3O) radical

$$Cl + c\text{-}C_2H_4O \rightarrow HCl + c\text{-}C_2H_3O$$
$$\Delta_r H_{298K} = -2 \pm 3 \text{ kcal mol}^{-1} \quad (2a)$$

The derivation of the thermochemistry of this and subsequent reactions was described in detail by Pearce et al.[21] The oxiranyl radical is a polar species, with a dipole moment computed at the MP2/6-311G(d,p) level of theory of 1.72 D. It is the least stable of the three possible C_2H_3O isomeric products; ring-opening reactions to produce the vinoxy (CH_2CHO) or acetyl (CH_3CO) radicals are significantly more exothermic

$$Cl + c\text{-}C_2H_4O \rightarrow HCl + CH_2CHO$$
$$\Delta_r H_{298K} = -35.4 \pm 0.9 \text{ kcal mol}^{-1} \quad (2b)$$

$$Cl + c\text{-}C_2H_4O \rightarrow HCl + CH_3CO$$
$$\Delta_r H_{298K} = -40.9 \pm 0.5 \text{ kcal mol}^{-1} \quad (2c)$$

The main pathway for reaction of Cl atoms with thiirane, the sulfur analogue of oxirane, is abstraction of the sulfur atom to form SCl and ethene,[38] with abstraction of an H atom constituting a minor (<30%) channel. The analogous O-atom abstraction for oxirane has not been observed experimentally, however, and calculations suggest too high a barrier to this reaction for it to occur under our experimental conditions.[39]

There are two chemically distinct sites for abstraction of H atoms from oxetane, leading to HCl and either of the oxetan-1-yl or oxetan-2-yl radicals, following abstraction at either of the two α-C atoms (adjacent to the oxygen atom) or the β-C atom

$$Cl + c\text{-}C_3H_6O \rightarrow HCl + \alpha\text{-}c\text{-}C_3H_5O$$
$$\Delta_r H_{298K} = -6.0 \text{ kcal mol}^{-1} \quad (3a)$$

$$Cl + c\text{-}C_3H_6O \rightarrow HCl + \beta\text{-}c\text{-}C_3H_5O$$
$$\Delta_r H_{298K} = -3.4 \text{ kcal mol}^{-1} \quad (3b)$$

The thermochemistry for reaction 3 is derived from electronic structure calculations with a thermal correction, because experimental data were unavailable. The two pathways were not resolved in prior measurements of HCl rotational excitation, but the experimentally derived HCl product rotational distribution for this reaction was found to be very similar to that from the reaction of Cl atoms with DME at a comparable collision energy.[21] The MP2/6-311G(d,p) computed dipole moments of the oxetan-1-yl and oxetan-2-yl radicals, 1.92 and 1.81 D, respectively, are, however, considerably higher than that of the CH_3OCH_2 product of the Cl + DME reaction (1.36 D), and the mean HCl rotational excitation lies below the value expected from dipole correlation arguments.[21]

The dynamics of reactions 2 and 3 are explored further here, with nascent HCl product detection by resonance-enhanced multiphoton ionization (REMPI) coupled with direct current (DC) slice velocity map imaging[27,28,40] to extract angular scattering distributions in the CM frame. The reactions were initiated by photodissociation of Cl_2, and the resultant HCl velocity map images were analyzed using a variant of the photoinitiated law of cosines (photoloc) method.[41] The photoloc procedure provides a direct link between the laboratory frame speeds of reaction products and the CM frame-scattering angle when the undetected coproduct of the reaction has no excess energy in its internal degrees of freedom. The radical coproducts of reactions 1−3 will, however, carry significant fractions of the available energy in their various rotational and vibrational modes, thus making the standard photoloc procedure unreliable. Brouard and co-workers developed a variant of the photoloc method, employing a Legendre moment analysis of velocity map images, that allows for the effects of a distribution of HCl CM frame velocities, arising from population of different internal states of the radical coproduct, on the measurable distribution of laboratory frame speeds.[26,32,33] This analysis method is employed here to derive CM frame distributions of scattering angles and product kinetic energies for reactions 2 and 3.

2. Method

A. Experimental Procedures. The experimental apparatus has been described in detail elsewhere.[34] In brief, it consisted of a velocity map imaging machine and two laser systems, with associated electronics for timing of gas and laser pulses and for data acquisition. The velocity map imaging spectrometer was constructed within a vacuum chamber with separately pumped source, TOF, and detector regions. The source region contained a late-mixing nozzle, ports fitted with quartz windows for laser beam access, and ion optics for velocity map imaging. The adjacent, field-free TOF region was maintained at ground potential; the final region housed the detector and could be isolated from the TOF and source regions by a manual gate valve.

Diluted reagent gases, Cl_2 (25% in Ar), oxirane (25% in Ar), or oxetane (17% in Ar), were stored in Teflon-lined, stainless steel cylinders at total pressures of 2.5 bar. The gases were introduced into the reaction chamber via a late-mixing nozzle assembly comprised of two separate 10-Hz pulsed valves, mounted on a polytetrafluoroethylene (PTFE) block through which narrow channels were bored to merge the two gas flows just prior to expansion into vacuum. Typical source chamber operating pressures of 8×10^{-6} Torr (when operating the nozzle for Cl_2 delivery) and 1.5×10^{-5} Torr (when also delivering the organic precursor) were used. The first electrode of the ion optics assembly (the repeller plate) was attached directly to the front of the PTFE block and was drilled with a narrow orifice that matched the aperture of the exit channel in the PTFE block at the point of contact. To optimize downstream number densities, the expansion of reagents was not skimmed. The repeller plate aperture was machined into a 40° cone, which increased molecular beam collimation significantly compared to a sonic nozzle. There was no evidence of clustering in the expansion under the experimental conditions used.

Cl_2 molecules were photolyzed by the third harmonic (355 nm wavelength) output of a Nd:YAG laser (Continuum Surelite), focused into the reaction chamber with an $f = 25$ cm quartz lens. This laser beam entered the chamber perpendicular to the TOF axis and passed through the center of the gap between the repeller and extractor plates. The electric vector of the light was vertically linearly polarized (with the polarization vector lying parallel to the face of the position-sensitive detector). Typical energies employed were <4 mJ per pulse at a 10-Hz repetition rate. The Cl_2 photolysis produced predominantly (>98%) ground spin orbit state $Cl(^2P_{3/2})$ atoms via a perpendicular transition ($\beta = -1$);[42,43] the co-reagent organic molecules did not absorb at this wavelength.[44] After a delay of 60 ns to allow for reaction, the nascent $HCl(v' = 0)$ products were probed by $2 + 1$ REMPI (via the $f^3\Delta_2 - X^1\Sigma^+$ (0,0) 2-photon excitation) with a counterpropagating, vertically linearly polarized, UV laser pulse, focused using an $f = 25$ cm lens. The wavelength of this laser beam was ~244 nm, generated by frequency doubling the fundamental (~10 mJ) output of a dye laser (Lumonics HD 500; Coumarin 480 dye) pumped by the third harmonic output of a Nd:YAG laser (Spectra Physics GCR 230). The probe laser beam energy was ~1 mJ per pulse in the UV at a 10-Hz repetition rate.

The Newton spheres of HCl^+ ions produced by REMPI of nascent HCl reaction products were extracted by a shallow electric field (68.3 V cm^{-1} between the repeller and extractor plates, 59.3 V cm^{-1} between the extractor and a third electrode serving as an electrostatic lens, and 142.3 V cm^{-1} between the lens and the entrance plate to the TOF tube). The shallow field allowed the sphere to elongate along the TOF axis while in the extraction region. After flight down the field-free TOF region, the cloud was sufficiently stretched in arrival times for DC slicing by pulsed gating of the detector.[28]

The ions of interest were detected by a pair of 75-mm diameter microchannel plates (MCPs) linked by a central tab and coupled to a P47 phosphor screen (Burle Electro-Optics). A short-duration (~50 ns), −500-V pulse to the front of the MCP assembly was used for DC slicing of the ion packet. The images of the products were recorded by a position-sensitive charge-coupled device camera (LaVision Imager Compact QE, 1390×1024 pixels, 12 bits). The camera was linked to a PC where images were accumulated using LaVision DAVIS software with real-time ion counting.[45] Images were accumulated while step scanning the laser over the full Doppler line width of the HCl transition, cycling over the transition typically 15 times. A step size of 0.02 cm^{-1} was used, with typical averaging over ~150 shots per step when detecting HCl products, and the signal was gated on analysis of the arrival of $m/z = 36$ ions. Approximately 30−40 thousand shots were accumulated per image depending on signal levels. Experimental timings of the photolysis and probe lasers, pulsed valves, and detection electronics were controlled using a delay generator (BNC 555) at a data acquisition rate of 10 Hz. From image analysis for HCl contaminant entrained in the pulsed gas expansion, the translational temperature of the gas mixture was determined to be 55 ± 5 K.

B. Analysis Method. The velocity map images were analyzed using the method of Brouard and co-workers,[26,32,33] which allows for a distribution of HCl speeds in the CM frame corresponding to the cofragment being formed with a range of internal energies. This method should be superior to standard photoloc analysis of the data[34,41] for reactions 1−3 because of the likelihood of deposition of significant fractions of the available energy into the numerous internal degrees of freedom of the coproduct radical.

Image analysis employed low order moments of the product LAB-frame speed and angular scattering distributions, which were extracted from experimental HCl ($v' = 0$, J') DC slice images. These low-order moments were fit to basis functions generated using the known energetics of the reaction under study, the experimentally determined translational beam temperature, and instrument velocity resolution. This latter parameter was determined from Cl atom images for Cl_2 photodissociation at 355 nm. The calculation of basis functions and the fitting were performed using programs written by Vallance and co-workers,[33] which were adapted for analysis of DC slice images with compensation for varying degrees of slicing of fast and slow products.[26,32,39] Legendre moments of the experimental images, $M_L^{exp}(v_{HCl})$, with $L = 0$ or 2, were calculated for all LAB-frame speeds, v_{HCl} (i.e., all image radii), by weighted integration of the image intensities over the polar angle within the image plane, φ

$$M_L^{exp}(v_{HCl}) = \frac{1}{2}\int_{-1}^{1} (2L+1) I(v_{HCl},\varphi) P_L(\cos\varphi) d\cos\varphi \quad (4)$$

These image moments were fit to a set of basis functions constructed using a distribution of CM frame-scattering angles (θ) and HCl speeds (u_{HCl}) that was taken to be of separable form. The CM frame functions were expressed as joint Legendre polynomial expansions in $\cos\theta$ and f'_t (with $f'_t = 2f_t - 1$, where f_t is the fraction of the available energy released as product translation), using the relationship between f_t and u_{HCl}. LAB-frame basis functions were then derived by coordinate transformation and Monte Carlo integration over the distribution of reagent velocities expected under the experimental conditions, followed by projection onto the plane of the imaging detector. This final step was adapted from the method of Brouard and co-workers[26] to limit the projection to the resolution of the speed component along the TOF axis appropriate for the experimental slice imaging. Fits to the LAB-frame basis functions employed a genetic algorithm based χ^2 minimization procedure. The analysis outputs were best-fit CM frame distributions $P(\cos\theta)$ and $P(f_t)$ together with simulated LAB frame Legendre moments of the images, $M_L^{fit}(v_{HCl})$, for comparison with the experimental data.

The numbers of Legendre polynomials in the CM frame expansions of the distributions in $\cos\theta$ and f_t were user-specified and were manually varied to obtain the best fits to experimental

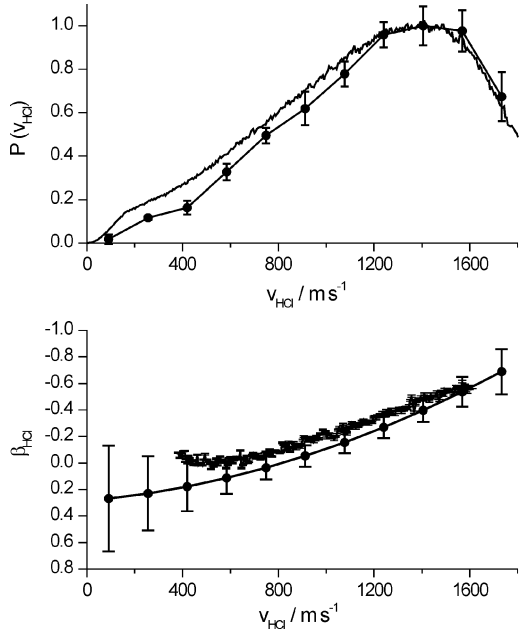

Figure 2. LAB speed distribution of the HCl($v' = 0$, $J' = 1$) products from the reaction of Cl($^2P_{3/2}$) + C_2H_6 shown in the upper panel compared with that measured by Zare and co-workers (black points).[12] The measured speed-dependent translational anisotropy parameter, β_{HCl}-(v_{HCl}), is shown in the lower panel and is again compared with that measured by Zare and co-workers (black points).

images. Basis functions constructed with $n = 3-4$ Legendre polynomials in cos θ and $m = 3-5$ in f_t were used in the fitting, and sets of these angular and radial functions are denoted hereafter as (n, m). The preferred values of n and m reflect the CM frame resolution of the experiment in cos θ and f_t.

3. Results

A. Test of the Analysis Method for the Cl + C_2H_6 Reaction. The fitting procedure was tested on the derivation of CM frame distributions of scattering angles and translational energy release for the products of reaction 1 under the photoinitiated conditions of our experiments, with a CM frame collision energy of 5.5 ± 1.5 kcal mol^{-1} (the uncertainty represents ±half width at half maximum of the collision energy distribution). The outcomes of crossed molecular beam experiments on this reaction are available at comparable collision energies for critical comparison.[37] Figure 2 shows the LAB speed distribution of the HCl($v' = 0$, $J' = 1$) products and the speed-dependent spatial anisotropy parameter for the product recoil, derived from velocity map images obtained while scanning the probe laser frequency over the full Doppler profile of the $R(1)$ line of the $f\,^3\Delta_2 - X\,^1\Sigma^+$ (0,0) transition. These data agree well with previous core-extracted TOF measurements by Kandel et al.[5] Small discrepancies at lower speeds may result from overdetermination of slow products in our experiment because of imperfect DC velocity slicing and some residual HCl contamination in the expanded gas mixture, both of which are allowed for in the analysis.

A typical velocity map image and the extracted zeroth- and second-order experimental LAB-frame Legendre moments of the HCl($v' = 0$, $J' = 1$) products from the Cl + C_2H_6 reaction are shown in Figure 3 along with fits using the (3, 3) set of calculated basis functions. This number of angular and radial functions was found to give the best fit to the experimental data and is limited by factors such as the velocity resolution of the experiment. The CM frame angular scattering and translational

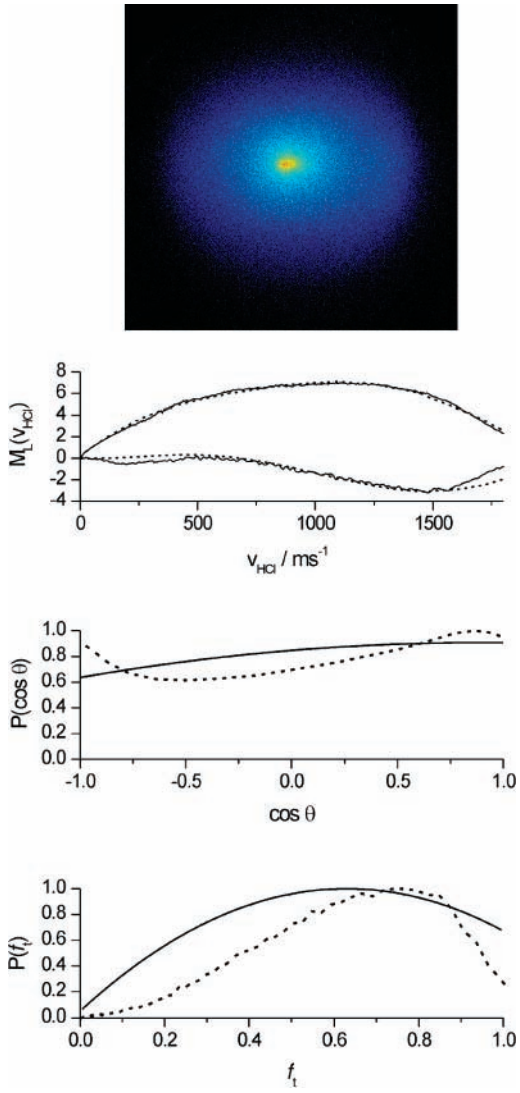

Figure 3. Top panel: a representative velocity map image for HCl(v' = 0, J' = 1) products of reaction of Cl atoms with ethane. Second panel: the speed-dependent zeroth- and second-order experimental Legendre moments of the image (solid lines) together with fits to calculated basis functions (dotted lines). Third panel: the CM frame angular distribution of HCl($v' = 0$, $J' = 1$) products derived from the fits (solid line) is compared with that measured by Suits and co-workers (dashed line) using a CMB setup at the higher collision energy of 6.7 kcal mol^{-1}.[37] Bottom panel: the fractional translational energy release distribution (solid line) is compared with that measured by Suits and co-workers (dashed line).

energy release distributions (P(cos θ) and $P(f_t)$, respectively) obtained from the fits are shown in the lower panels of Figure 3 and are compared to those measured by Suits and co-workers in a CMB apparatus.[37] The angular scattering distributions are in satisfactory agreement, with broad, slightly forward peaked scattering in the CM frame; discrepancies at large and small scattering angles are most likely to be a consequence of the lower angular resolution of our experiment. The LAB speed resolution not only affects the CM frame angular resolution but also has consequences for the retrieval of $P(f_t)$. As Figure 3 shows, our experiments and analysis capture the general form of $P(f_t)$ but not the finer details of the results of the crossed molecular beam data.

Table 1 compares the average f_t for products, as derived from the fits, with those obtained by other methods. In the current work, $\langle f_t \rangle$ was deduced from the values of $\Delta_r H_{298\ K}$, the mean collision energy, and the average rotational energy of HCl

TABLE 1: Mean Fractional Translational Energy Release for the Products of Reaction of Cl Atoms with Ethane at a CM Frame Collision Energy of 5.5 ± 1.5 kcal mol^{-1} and Mean Internal Energy of the Ethyl Radical Products Formed with HCl($v' = 0$, $J' = 1$) (Errors in $\langle f_t \rangle$ and $\langle f_{int}(C_2H_5) \rangle$ Are Estimated as ±0.20, Arising Primarily from the Spread in the Collision Energy; Values Are Compared with Results of Other Studies at Comparable Collision Energies)

method	$\langle f_t \rangle$	$\langle f_{int}(C_2H_5) \rangle$
Legendre moment fitting (this work)	0.57	0.42
photoloc analysis	0.75	0.24
crossed molecular beams[a]	0.63	0.35
trajectory calculations[b]	0.78	0.21
Legendre moment fitting (ref 26)	0.80	0.19

[a] From ref 37 for HCl($v' = 0$, $J' = 2$), with experiments at a collision energy of 5.3 kcal mol^{-1}. [b] From ref 39 with data averaged over all HCl($v' = 0$) rotational levels.

coproducts, which are mostly formed in $v' = 0$ and low J' levels. Fits with larger numbers of moments in f_t ($m \geq 4$) introduced overly oscillatory forms for $P(f_t)$, with a sharp peak at $f_t \approx 1$ and a second peak at $f_t \approx 0.2-0.4$. The uncertainties in $\langle f_t \rangle$ and the values of the fraction of the available energy becoming radical internal energy ($f_{int}(R)$) are typically ±0.20, deriving from the spread in the collision energy (the main source of uncertainty in the energetics). The equivalent values determined from a standard photoloc analysis of the data are also presented in Table 1,[41,46] together with the values determined by Suits and co-workers from their CMB measurements, those of Rudić et al. from trajectory calculations,[16] and those from Brouard and co-workers using a method similar to the current experiments and analysis.[26] The $\langle f_t \rangle$ and $\langle f_{int}(C_2H_5) \rangle$ values from the current study show better agreement with the values determined from CMB experiments than do the results of the standard photoloc analysis.

B. Cl + *c*-C_2H_4O Reaction. Velocity map ion images were recorded of the nascent HCl($v' = 0$, J') products from reaction 2 at a collision energy of 6.5 ± 1.5 kcal mol^{-1}, while scanning the probe laser frequency over the full Doppler profile of the $S(0)$, $R(1)$, or $R(2)$ lines of the $f\,^3\Delta_2 - X\,^1\Sigma^+$ (0,0) transition. A representative image is shown in Figure 4. Images for higher HCl rotational states were not measured because of low signal levels arising from the cold rotational level population distribution.[21] In all cases, the LAB speed distributions of the HCl products were consistent with the energetics of abstraction of H from oxirane to form HCl and the cyclic oxiranyl radical, and it was not necessary to invoke the more exothermic ring-opening channels.

As for analysis of images for the products of reaction 1, low-order, LAB-frame Legendre moments were extracted from the DC slice images of HCl($v' = 0$, $J' = 2$) from reaction 2 and fit using (3,3), (4,4), and (3,5) sets of basis functions. The extracted zeroth- and second-order experimental Legendre moments of the HCl($v' = 0$, $J' = 2$) products from the Cl + *c*-C_2H_4O reaction are shown in Figure 4, along with fits using the (3, 5) set of calculated basis functions. There is some contaminant HCl present at very low speeds, but the fitting was otherwise satisfactory. The derived distributions of CM frame-scattering angles and translational energy release for the products are plotted in the lower panels of the figure. We obtained an angular distribution of HCl($v' = 0$, $J' = 2$) products that is broad and slightly forward−backward peaking in the CM frame. The outcomes for $J' = 0$ and 1 were very similar. These results are reminiscent of measurements by Murray et al. for the Cl + CH_3-OH and Cl + CH_3OCH_3 reactions.[18] Using more than three

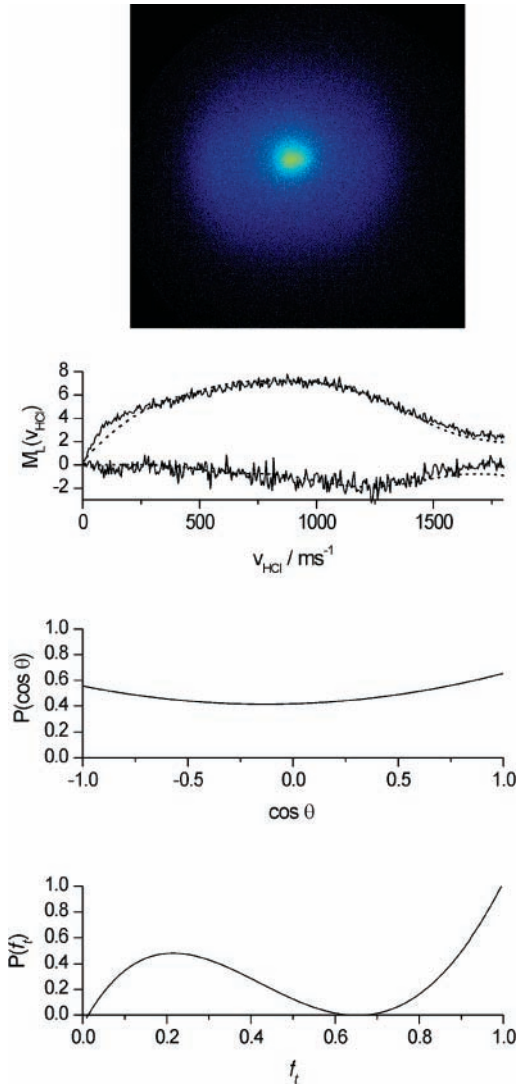

Figure 4. Top panel: a velocity map image of the HCl($v' = 0$, $J' = 2$) products of the Cl + *c*-C_2H_4O reaction. Second panel: the zeroth- and second-order experimental Legendre moments derived from the image (solid lines) and fits to calculated basis functions (dotted lines). The CM frame angular scattering distribution and fractional translational energy release for HCl($v' = 0$, $J' = 2$) products are plotted, respectively, in the third and fourth panels.

angular moments in the fit introduced implausible oscillatory angular structure in the derived angular scattering distribution. The largest sources of error in the derived angular scattering distributions are the uncertainty in the reaction energetics and the variability in the outcomes of fits employing different (n, m) basis sets, which outweigh error estimates based on reproducibility of the measurements. As a result, we are unable to place meaningful error bars on the $P(\cos\,\theta)$ distribution plotted in Figure 4, and note that there is also uncertainty in the angular resolution of the data. We therefore draw only a general conclusion that the CM frame scattering is broad, and forward−backward peaking for the HCl products of reaction 2.

The form for $P(f_t)$ obtained from fits with different numbers of radial functions is variable, with a small basis set ($m = 3$) giving a wide distribution but a poor fit to the experimental zeroth-order moment (the LAB speed distribution), whereas $m = 4$ and 5 basis sets resulted in near-identical $P(f_t)$ distributions of the type plotted in Figure 4, showing what we believe to be an unlikely bimodality in the outcome. Some of the variability in the fit outcomes may stem from an imprecise knowledge of

TABLE 2: Mean Fractional Translational Energy Release for the Products of Reaction of Cl Atoms with *c*-C_2H_4O at a CM Frame Collision Energy of 6.5 ± 1.5 kcal mol^{-1} and Mean Internal Energy of the Oxiranyl Radical Coproduct Formed with HCl($v' = 0$, $J' = 2$) (Values Are Calculated Using the Reaction Energetics Specified in Eq 2a, with Uncertainties of ±0.18 Derived from the Spread of Collision Energies)

method	$\langle f_t \rangle$	$\langle f_{int}(c\text{-}C_2H_3O) \rangle$
Legendre moment fitting	0.52	0.47
photoloc analysis	0.55	0.44
trajectory calculations[a]	0.38	0.48

[a] From ref 39 with data averaged over all HCl($v' = 0$) rotational levels.

the value of $\Delta_r H_{298K}$. There are thus considerable uncertainties in the correct form for the distribution of f_t for reaction 2, and we instead focus on mean values for f_t from this study which are summarized in Table 2, together with outcomes of the standard photoloc analysis of our data and previously reported trajectory calculations. The amounts of available energy channelled into the radical internal energy, as determined from the Legendre moment fitting procedure and the standard photoloc analysis, are in good agreement at ~46%. This outcome is very similar to the fractions of the available energy that become internal energy of the radical products from the reactions of Cl + CH_3OH (49%) and Cl + CH_3OCH_3 (46%).[18]

C. Cl + *c*-C_3H_6O Reaction. At a CM frame collision energy of 7.3 ± 1.6 kcal mol^{-1}, velocity map images recorded for the nascent HCl($v' = 0$, J') products from the reaction of Cl atoms with *c*-C_3H_6O showed the highest signal levels for $J' = 3$ and 4. Images of HCl ($v' = 0$, $J' = 0-2$) contained unwanted signal at the center from contaminant HCl entrained in the pulsed expansion. Measurements at higher J' were hampered by low signal levels and a rising background from nonresonant ionization and fragmentation of the oxetane molecule.

The LAB speed distributions of the HCl product, ranging from 0−2000 m s^{-1}, were energetically consistent with contributions from either α- or β-H abstraction channels to form HCl with, respectively, the cyclic oxetan-1-yl and oxetan-2-yl radicals. For abstraction of an α-H atom, the expected minimum and maximum HCl($v' = 0$, $J' = 4$) LAB speeds, assuming no energy imparted to the radical internal modes, are 790 and 2050 m s^{-1}. Increasing internal excitation of the radical reduces both the minimum and maximum speeds, and the former can become zero. For β-H atom abstraction, the corresponding maximum speed is 1670 m s^{-1}.

Zeroth- and second-order LAB moments were extracted from the DC slice images of product HCl($v' = 0$, $J' = 4$) from the reaction of Cl + *c*-C_3H_6O. Basis functions constructed from (3,3), (4,4), and (3,5) sets of Legendre functions were tested for the fitting. Analysis was performed using basis functions that assumed each of the following three possibilities: (i) abstraction of H atoms only from α-C atoms; (ii) abstraction only from β-C atoms; (iii) abstraction from both α- and β-C atoms with adjustable weights. The outcomes of these fits are contrasted below.

Fits to the* α-*H or* β-*H Abstraction Channel. The data were first fit with basis functions calculated for the α-H atom abstraction channel of the reaction, using the energetics specified in eq 3a. The fitting was generally good for the (4,4) and (3,5) basis sets but poor for the (3,3) fit to the second moment. Small discrepancies at very high product LAB speeds were most likely to be a consequence of a rising background signal.[47] The angular distribution of HCl($v' = 0$, $J' = 4$) products was determined to be broad and forward−backward peaking in the CM frame for all fits, and the results were consistent regardless of the number of basis functions used. The derived distribution of f_t was also broad and peaked around 0.3−0.4.

The fits to basis functions constructed for the β-H abstraction channel were generally not as good as for the α-H atom abstraction channel, as exemplified by higher χ^2 values, with discrepancies greatest at high product speeds. The returned CM frame angular scattering distributions were again broad and forward−backward peaking, closely resembling those derived from the α-H abstraction channel fitting. The distribution of fractional translational energy release was also wide, but peaked at $f_t \approx 1$ for two of the sets of fitting functions because high kinetic energy release is required to account for the fastest LAB frame products when using the lower exothermicity of the β-abstraction channel. It is likely that these products originate instead from the more exothermic α-H abstraction channel.

Simultaneous Fits to Both* α-*and* β-*H Abstraction Channels. Fits of the experimental moments to basis functions representing competitive reaction via both the α- and β-H abstraction channels allowed the relative contribution of each reaction channel to be estimated. The angular scattering and fractional kinetic energy distributions were constrained to be the same for the two channels using this analysis, but the overall forms were varied. These constraints significantly reduced the required number of fitting parameters, and a similar approach was previously employed by Brouard and co-workers in their analysis of data from the Cl + *n*-C_4H_{10} reaction.[32] They reported no significant difference in χ^2 values when fitting with CM frame angular scattering and f_t distributions constrained to be the same for both primary and secondary H-atom reaction channels or when allowing them to differ.

A representative image and the extracted zeroth- and second-order experimental Legendre moments of the HCl($v' = 0$, $J' = 4$) product velocities from the Cl + *c*-C_3H_6O reaction are shown in Figure 5 along with fits using the combined α- and β-H abstraction basis functions. The quality of the fit (as measured by χ^2 values) was clearly better for the simultaneous fitting to both channels than for the β-H abstraction channel fit and is a slight improvement on the fit to only the α-H abstraction channel. The returned scattering distributions are also shown in the figure and again show forward−backward peaked product scattering in the CM frame. The same cautionary comment that was made in section 3B also applies to the uncertainties in the plotted $P(\cos\theta)$ values and the angular resolution in $\cos\theta$. As was noted earlier for the results for reaction 2, the $P(\cos\theta)$ outcome is very similar to the measurements by Murray et al. for HCl from the Cl + CH_3OH and Cl + CH_3OCH_3 reactions in a parallel molecular beam setup, suggesting comparable H atom abstraction dynamics.[18] The fractional translational energy release distribution is wide, indicating varied levels of internal excitation of the radical coproduct, and peaks at $f_t \approx 0.5$.

The fits were optimized with a 63 ± 10% contribution from the α-H abstraction channel and 37 ± 10% contribution from the β-H abstraction channel. Given the 2:1 abundance of α-H to β-H atoms in oxetane, this result suggests there is an approximately equal propensity for abstraction of either type of H atom, at least for the formation of HCl($v' = 0$, $J' = 4$). The internal energy of the HCl products was used in energy balance arguments to determine the fractional internal energy of the oxetan-1-yl and oxetan-2-yl radicals. Table 3 presents the derived mean fractional energy release into translation of the products for the α- and β-H abstraction channels and the fractional internal energy of the oxetan-1-yl and oxetan-2-yl radicals. The uncertainties in the values of $\langle f_t \rangle$ and $\langle f_{int}(c$-

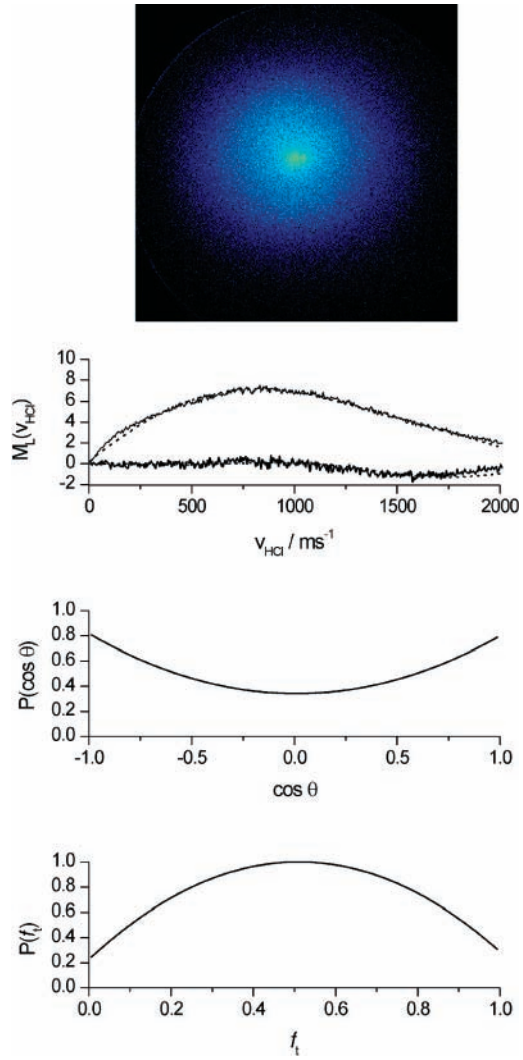

Figure 5. Top panel: a velocity map image of the HCl($v' = 0$, $J' = 4$) products of the Cl + c-C_3H_6O reaction. Second panel: zeroth- and second-order experimental Legendre moments of the image (solid lines) together with fits to the moments using basis functions calculated for the α- and β-H abstraction channels (dotted lines). The lower two panels show the resultant CM frame angular scattering and fractional translational energy release distributions for HCl($v' = 0$, $J' = 4$) reaction products.

TABLE 3: Mean Fractional Translational Energy Release for the Products of the Cl + c-C_3H_6O Reaction at a CM Frame Collision Energy of 7.3 ± 1.6 kcal mol^{-1} and Mean Internal Energies of the Oxetan-1-yl and Oxetan-2-yl Radical Coproducts Formed with HCl($v' = 0$, $J' = 4$) (Values Are Calculated Using the Reaction Energetics Specified in Eq 3, with Uncertainties of ±0.12 Derived from the Spread of Collision Energies)

	α-H abstraction		β-H abstraction	
method	$\langle f_t \rangle$	$\langle f_{int}(c\text{-}C_3H_5O) \rangle$	$\langle f_t \rangle$	$\langle f_{int}(c\text{-}C_3H_5O) \rangle$
Legendre moment fitting	0.54	0.42	0.54	0.41
trajectory calculations[a]	0.31	0.66	0.36	0.47

[a] From ref 39 with data averaged over all HCl($v' = 0$) rotational levels.

$C_3H_5O)\rangle$ are ±0.12 for the α- and β-H abstraction channels, arising from the spread of collision energies; the reaction enthalpy values used come from ab initio calculations, and we cannot attach a reliable uncertainty to them. The average amounts of available energy channelled into the internal energy of the oxetan-1-yl and oxetan-2-yl radicals are determined to be very similar for all the fitting procedures and are comparable to the fraction of the available energy that becomes internal energy of the radical products from the reactions of Cl + CH_3-OH and Cl + CH_3OCH_3.[18]

For the Cl + c-C_3H_6O reaction, the derived CM frame-scattering distributions are largely invariant to whether the fit assumes α- or β-H abstraction or allows for both channels simultaneously. As was noted above, the f_t distributions show some variation with analysis method, which can be understood in terms of the different exothermicities for the two channels. There is thus greater confidence in the outcomes of the fits, as plotted in Figure 5, compared to those for the Cl + c-C_2H_4O reaction (Figure 4).

4. Discussion

The CM frame-scattering distributions for products of reactions 1−3 all show broad scattering in the CM frame and wide ranges of kinetic energy release, indicating a distribution of internal energies of the radical coproduct. Calculations of the potential energies along the reaction paths indicate that there are no wells on the PESs for these reactions that have depths sufficient for the support of long-lived complexes. The scattering over all CM frame angles is instead interpreted as indicative of successful reactive collisions over a wide range of impact parameters: small impact parameters lead to rebound dynamics and backward scatter, whereas reactions at larger impact parameters, corresponding to approach of Cl atoms to the periphery of the organic molecule, give sideways and forward scattering. This interpretation is consistent with there being a low or nonexistent barrier to reaction (see Figure 1) and a slow rise in potential energy with the Cl−H−C bending angle, as deduced from the previously calculated low frequency bending modes at the transition state.[21] There are therefore few steric restrictions to reaction over a wide range of approach geometries of the Cl atoms.

The computed stationary points on the potential energy surfaces for reactions 2 and 3 bear close resemblance to those previously calculated for the reactions of Cl atoms with the noncyclic CH_3OH and CH_3OCH_3 molecules,[14] and the similar forms for the CM frame angular scattering for all these abstraction reactions suggest comparable scattering dynamics. The results presented here thus do not show any signs of differences in reaction dynamics for cyclic and noncyclic ethers and alcohols, unlike the outcomes of our previous measurements of the extent of rotational excitation of the HCl($v' = 0$, J') reactions products. The differences in the populations of rotational levels of the HCl were attributed to interactions between the polar HCl and radical coproducts in the post-TS region of the PES and the differences between reorientational motion of (near-oblate) cyclic and (rodlike) noncyclic radical products on the time scale of separation from the HCl.[2,22] The scattering dynamics captured in the angular distributions plotted in Figures 3−5 are largely determined by the ranges of impact parameters that lead to reaction (the reaction opacity functions), which are features of the approach to the TS region and thus most sensitive to the pre-TS part of the PES. The post-TS interactions are thus unlikely to play a role in determining the scattering angle distribution but may induce transitions between rotational levels of the nascent HCl through torques induced by long-range electrostatic interactions as the products separate. Although different impact parameter collisions might initially favor formation of HCl in low or higher J' levels (e.g., rebound dynamics associated with small impact parameters may cause more impulsive energy release and thus greater HCl rotational excitation), these post-TS torques will blur differences between

the angular scattering distributions for the asymptotic HCl(J') products, as was discussed previously for the reaction of Cl with CH_3OH.[18] This deduction is borne out by the similarities of the $P(\cos\theta)$ distributions for HCl($v'=0$, J') in different J' levels for each of reactions 2 and 3.

There is some uncertainty in the products of reaction 2 because of the possibility of ring-opening dynamics leading to the strongly exothermic production of vinoxy or acetyl radicals. The laboratory frame speed distributions of the HCl products from the reaction of Cl with oxirane, as determined from DC slice images, show no indication of the release as translational energy of the additional exothermicity associated with vinoxy or acetyl radical formation. The radial dependence of the images can be fully accounted for by the thermodynamics of reaction 2a, but we cannot entirely discount the formation of vinoxy or acetyl radicals with large amounts of internal excitation, either as a direct product of the reaction or by ring opening of internally energized oxiranyl radicals after the abstraction process.

Analysis of the data for reaction 3 of Cl atoms with oxetane suggests an ~2:1 contribution from the α- and β-H abstraction channels, consistent with the branching being determined primarily by the number of H atoms occupying each site in the oxetane molecule. Previous experimental data and direct dynamics trajectory calculations suggested that the α- and β-H abstraction channels, respectively, would result in low and higher levels of HCl rotational excitation. Figure 6 illustrates the origins of these effects: the rotational motion induced in the oxetanyl radical upon separation from the TS is about a different axis for α- and β-H, with only the latter favoring reorientation of the O-atom into an attractive interaction with the departing HCl. A 2:1 propensity for the two channels can thus account for the overall distribution of HCl molecules over rotational levels, which favors lower J' quantum numbers to a greater extent than expected from correlations derived for Cl atom reactions with noncyclic polyatomic molecules.[17] We can simulate the combined effects of the α- and β-H abstraction channels by co-adding a component for the α-H channel (for which radical reorientation dynamics do not lead to enhanced HCl rotation) mimicked by the cold experimental rotational distribution of HCl ($v'=0$, J') obtained from the Cl + c-C_2H_4O reaction, and a rotationally hotter component for the β-H abstraction channel (for which radical reorientation can enhance HCl rotation) represented by the HCl rotational distribution from the Cl + CH_3OH reaction. Figure 6 illustrates schematically the likely reorientation dynamics of the oxiranyl and hydroxymethyl radicals from these two reactions and compares them to those for the α- and β-H abstraction channels from oxetane. In these simple pictures, the dissociation of the TSs for the Cl + β-C_3H_6O and Cl + CH_3OH reactions induces radical rotation that reorients the radical O atom toward the departing HCl, thus inducing HCl rotation by an attractive interaction. The equivalent rotations of the oxetan-1-yl and oxiranyl radicals do not have the same effect. When the simulation procedure for the HCl rotational distribution is carried out for reaction 3, using data from the Cl + c-C_2H_4O and Cl + CH_3OH reactions as proxies for α- and β-H abstraction, and by application of a 2:1 population weighting, the composite rotational distribution plotted in Figure 6 is obtained. A small shift was applied to the rotational temperature of the HCl products from the Cl + CH_3-OH reaction to account correctly for the larger dipole moment of the oxetan-2-yl radical compared to that of hydroxymethyl. The composite distribution is compared with that obtained experimentally for reaction 3, and apart from counterbalancing discrepancies at $J'=1$ and 2, the two data sets are in good agreement. Fits to Boltzmann distributions give respective rotational temperatures of 399 ± 23 and 412 ± 16 K for the experimental data for reaction 3 and the composite distribution. These comparisons provide further weight to the argument for two reaction channels contributing to the distribution of products from reaction 3.

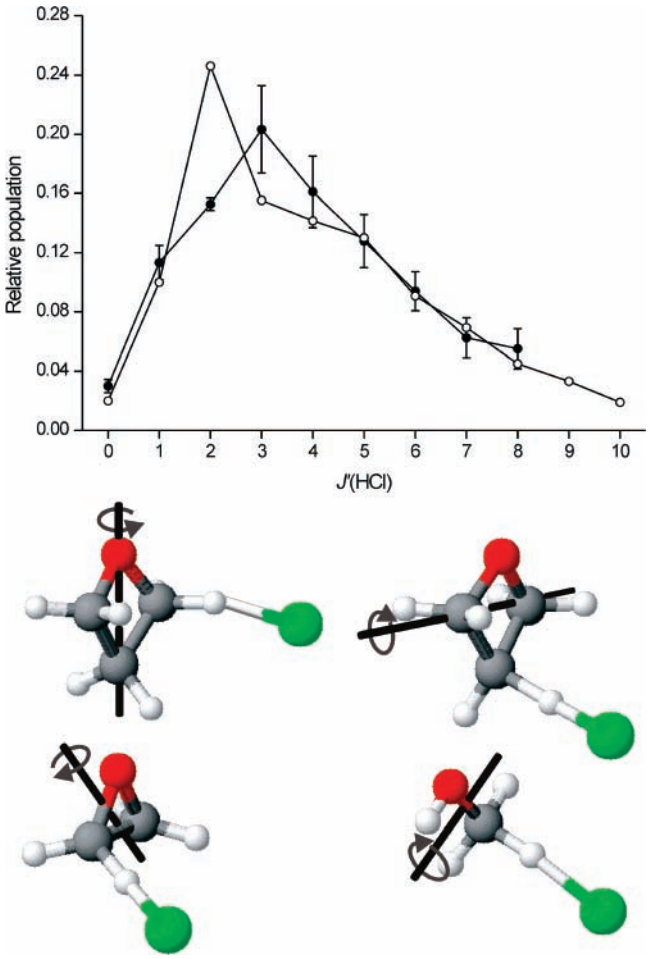

Figure 6. The HCl ($v'=0$, J') rotational distribution obtained experimentally for the Cl + c-C_3H_6O reaction (black circles) compared with a distribution obtained from the 2:1 combination of the experimental rotational distributions of the Cl + c-C_2H_4O and Cl + CH_3OH reactions (white circles). The molecular structures show the expected rotational motions of the radical products induced by separation from the transition state. Top row: α- and β-H abstraction from oxetane. Bottom row: abstraction of H from oxirane and methanol. Only dissociation of the two TSs in the right-hand column causes radical reorientation that favors approach of the O atom to the HCl and thus enhanced HCl rotation.

5. Conclusions

The reactions of photolytically generated, ground-state Cl atoms with ethane, oxirane (c-C_2H_4O), and oxetane (c-C_3H_6O) were studied by DC slice velocity map ion imaging of the HCl-($v'=0$, J') products, combined with analysis using a Legendre moment fitting technique. The derived CM frame angular scattering distribution for the HCl($v'=0$, $J'=1$) products from the reaction of Cl + C_2H_6 is in satisfactory agreement with that determined by Suits and co-workers from a crossed molecular beam experiment at a similar collision energy.[37]

A broad, forward, and backward peaking CM frame angular distribution of HCl products was determined for the reaction of Cl atoms with oxirane. The average fraction of the available

energy released as product translational energy was derived to be $\langle f_t \rangle$, equal to 0.52 ± 0.18, with the bulk of the remaining energy entering the rotational and vibrational modes of the radical coproduct, giving $+f_{int}(c\text{-}C_2H_3O) = 0.47 \pm 0.18$.

The evidence from scattering distributions, kinetic energy release data, and rotational excitation of HCl points to the occurrence of two competing channels for the reaction of Cl atoms with oxetane, corresponding to the abstraction of H atoms from positions either α or β to the O atom. The contributions from these two channels were estimated to be 63 and 37%, consistent with a statistical branching ratio. The angular scatter of HCl($v' = 0$) products in the CM frame is forward−backward peaking and broad, and the derived mean fractions of the available energy channelled into product translation and internal excitation are $\langle f_t \rangle = 0.54 \pm 0.12$ and $\langle f_{int}(c\text{-}C_3H_5O) \rangle = 0.42 \pm 0.12$. Under our experimental conditions, any variations in these distributions for the α- and β-H abstraction channels are indistinguishable.

The broad and forward−backward peaking CM frame angular scattering distributions of products for both reactions with cyclic ethers are very similar to those derived by an alternative experimental method for the reactions of Cl atoms with CH_3OH and CH_3OCH_3.[18] The broad product scattering is attributed to reactive collisions over a wide range of impact parameters, as might be expected for barrierless reactions with loose transition states. Such dynamics appear to be common to both cyclic ethers and noncyclic ethers and alcohols. Dynamical differences arising from the constrained cyclic geometries of oxirane and oxetane do, however, appear to be observable in the rotational excitation of the HCl coproducts.[21] The degree of rotation of the HCl can be accounted for by consideration of the polarity and the reorientation dynamics of the radical coproduct, which depend on molecular shape and reaction pathway. These reactive systems thus appear to demonstrate how the shape of a polyatomic molecule can influence its reaction dynamics, but for these H-atom abstraction reactions of Cl atoms with organic molecules, the dynamically important differences between linear and cyclic compounds arise in the post-TS region rather than in the approach to the TS.

Acknowledgment. The authors are grateful to Prof. M. Brouard and Dr. R. Cireasa (University of Oxford) for providing the original image analysis programs and Prof. A.G. Suits (Wayne State University) and Prof. R.N. Zare (Stanford University) for supplying data for comparison with some of the results presented here. We acknowledge financial support from the EPSRC through the Portfolio Partnership grant LASER (GR/S71750/01). B.R. thanks the European Commission for funding through the PICNIC IHP network HPRN-CT-2002-00183, and A.J.O.E. gratefully acknowledges a Royal Society and Wolfson Foundation Research Merit Award.

References and Notes

(1) Murray, C.; Orr-Ewing, A. J. *Int. Rev. Phys. Chem.* **2004**, *23*, 435.
(2) Murray, C.; Pearce, J. K.; Rudić, S.; Retail, B.; Orr-Ewing, A. J. *J. Phys. Chem. A* **2005**, *109*, 11093.
(3) Park, J. H.; Lee, Y. S.; Hershberger, J. F.; Hossenlopp, J. M.; Flynn, G. W. *J. Am. Chem. Soc.* **1992**, *114*, 58.
(4) Simpson, W. R.; Orr-Ewing, A. J.; Zare, R. N. *Chem. Phys. Lett.* **1993**, *212*, 163.
(5) Kandel, S. A.; Rakitzis, T. P.; Lev-On, T.; Zare, R. N. *J. Chem. Phys.* **1996**, *105*, 7550.
(6) Varley, D. F.; Dagdigian, P. J. *J. Phys. Chem.* **1995**, *99*, 9843.
(7) Varley, D. F.; Dagdigian, P. J. *J. Phys. Chem.* **1996**, *100*, 4365.
(8) Yoon, S.; Henton, S.; Zivkovic, A. N.; Crim, F. F. *J. Chem. Phys.* **2002**, *116*, 10744.
(9) Yoon, S.; Holiday, R. J.; Crim, F. F. *J. Chem. Phys.* **2003**, *119*, 4755.
(10) Blank, D. A.; Hemmi, N.; Suits, A. G.; Lee, Y. T. *Chem. Phys.* **1998**, *231*, 261.
(11) Hemmi, N.; Suits, A. G. *J. Chem. Phys.* **1998**, *109*, 5338.
(12) Kandel, S. A.; Rakitzis, T. P.; Lev-On, T.; Zare, R. N. *J. Phys. Chem. A* **1998**, *102*, 2270.
(13) Rudić, S.; Ascenzi, D.; Orr-Ewing, A. J. *Chem. Phys. Lett.* **2000**, *332*, 487.
(14) Rudić, S.; Murray, C.; Ascenzi, D.; Anderson, H.; Harvey, J. N.; Orr-Ewing, A. J. *J. Chem. Phys.* **2002**, *117*, 5692.
(15) Rudić, S.; Murray, C.; Harvey, J. N.; Orr-Ewing, A. J. *Phys. Chem. Chem. Phys.* **2003**, *5*, 1205.
(16) Rudić, S.; Murray, C.; Harvey, J. N.; Orr-Ewing, A. J. *J. Chem. Phys.* **2004**, *120*, 186.
(17) Murray, C.; Retail, B.; Orr-Ewing, A. J. *Chem. Phys.* **2004**, *301*, 239.
(18) Murray, C.; Orr-Ewing, A. J.; Toomes, R. L.; Kitsopoulos, T. N. *J. Chem. Phys.* **2004**, *120*, 2230.
(19) Toomes, R. L.; van den Brom, A. J.; Kitsopoulos, T. N.; Murray, C.; Orr-Ewing, A. J. *J. Phys. Chem. A* **2004**, *108*, 7909.
(20) Retail, B.; Pearce, J. K.; Murray, C.; Orr-Ewing, A. J. *J. Chem. Phys.* **2005**, *122*.
(21) Pearce, J. K.; Murray, C.; Stevens, P. N.; Orr-Ewing, A. J. *Mol. Phys.* **2005**, *103*, 1785.
(22) Pearce, J. K.; Murray, C.; Orr-Ewing, A. J. *Phys. Scripta* **2006**, *73*, C14.
(23) Eppink, A. T. J. B.; Parker, D. H. *Rev. Sci. Instrum.* **1997**, *68*, 3477.
(24) Chandler, D. W.; Houston, P. L. *J. Chem. Phys.* **1987**, *87*, 1445.
(25) Ahmed, M.; Peterka, D. S.; Suits, A. G. *Phys. Chem. Chem. Phys.* **2000**, *2*, 861.
(26) Bass, M. J.; Brouard, M.; Vallance, C.; Kitsopoulos, T. N.; Samartzis, P. C.; Toomes, R. L. *J. Chem. Phys.* **2003**, *119*, 7168.
(27) Lin, J. J.; Zhou, J. G.; Shiu, W. C.; Liu, K. P. *Rev. Sci. Instrum.* **2003**, *74*, 2495.
(28) Townsend, D.; Minitti, M. P.; Suits, A. G. *Rev. Sci. Instrum.* **2003**, *74*, 2530.
(29) Ashfold, M. N. R.; Nahler, N. H.; Orr-Ewing, A. J.; Vieuxmaire, O. P. J.; Toomes, R. L.; Kitsopoulos, T. N.; Garcia, I. A.; Chestakov, D. A.; Wu, S. M.; Parker, D. H. *Phys. Chem. Chem. Phys.* **2006**, *8*, 26.
(30) Toomes, R. L.; Kitsopoulos, T. N. *Phys. Chem. Chem. Phys.* **2003**, *5*, 2481.
(31) Ahmed, M.; Peterka, D. S.; Suits, A. G. *Chem. Phys. Lett.* **2000**, *317*, 264.
(32) Bass, M. J.; Brouard, M.; Vallance, C.; Kitsopoulos, T. N.; Samartzis, P. C.; Toomes, R. L. *J. Chem. Phys.* **2004**, *121*, 7175.
(33) Bass, M. J.; Brouard, M.; Cireasa, R.; Clark, A. P.; Vallance, C. *J. Chem. Phys.* **2005**, *123*, 094301.
(34) Retail, B.; Greaves, S. J.; Pearce, J. K.; Rose, R. A.; Orr-Ewing, A. J. *Phys. Chem. Chem. Phys.* **2007**, *9*, 3261.
(35) Zhou, J. G.; Lin, J. J.; Shiu, W. C.; Liu, K. P. *Phys. Chem. Chem. Phys.* **2006**, *8*, 3000.
(36) Li, W.; Huang, C. S.; Patel, M.; Wilson, D.; Suits, A. G. *J. Chem. Phys.* **2006**, *124*, 011102.
(37) Huang, C. S.; Li, W.; Suits, A. G. *J. Chem. Phys.* **2006**, *125*, 121101.
(38) Murrells, T. P. *J. Chem. Soc., Faraday Trans. 2* **1988**, *84*, 67.
(39) Pearce, J. K. Ph.D. Thesis, University of Bristol, 2007.
(40) Gebhardt, C. R.; Rakitzis, T. P.; Samartzis, P. C.; Ladopoulos, V.; Kitsopoulos, T. N. *Rev. Sci. Instrum.* **2001**, *72*, 3848.
(41) Shafer, N. E.; Orr-Ewing, A. J.; Simpson, W. R.; Xu, H.; Zare, R. N. *Chem. Phys. Lett.* **1993**, *212*, 155.
(42) Matsumi, Y.; Tonokura, K.; Kawasaki, M. *J. Chem. Phys.* **1992**, *97*, 1065.
(43) Samartzis, P. C.; Bakker, B. L. G.; Rakitzis, T. P.; Parker, D. H.; Kitsopoulos, T. N. *J. Chem. Phys.* **1999**, *110*, 5201.
(44) Talrose, V.; Yermakov, A. N.; Usov, A. A.; Goncharova, A. A.; Leskin, A. N.; Messineva, N. A.; Trusova, N. V.; Efimkina, M. V. webbook.nist.gov.
(45) Chang, B. Y.; Hoetzlein, R. C.; Mueller, J. A.; Geiser, J. D.; Houston, P. L. *Rev. Sci. Instrum.* **1998**, *69*, 1665.
(46) Simpson, W. R.; Orr-Ewing, A. J.; Rakitzis, T. P.; Kandel, S. A.; Zare, R. N. *J. Chem. Phys.* **1995**, *103*, 7299.
(47) Braun, A.; Drabbels, M. *Rev. Sci. Instrum.* **2005**, *76*, 113103.